Hittite Journal of Science and Engineering, 2018, 5 (1) 75-83
ISSN NUMBER: 2148-4171
DOI: 10.17350/HJSE19030000068

The Effect of Welding Positions on the Weldability of X20CrMoV11-1 Steels

Bünyamin Çiçek[1] Emine Gündoğdu İş[2] Emre Gümüş[2] Polat Topuz[2]
[1] Hitit University, Alaca Avni Celik Vocational School, Corum, TURKEY.
[2] Istanbul Gedik University, Gedik Vocational School, Istanbul, TURKEY.

ABSTRACT

In the study, mechanical properties of martensitic steel X20CrMoV11-1 was investigated after being welded using Tungsten Inert Gas (GTAW) welding method at different weld positions (PC and PJ-EN 6947). The X20CrMoV11-1 steels have been widely used in thermal power plant applications in combustion chambers and other high-temperature parts. These materials experience extremely high internal pressure at the service conditions. WCrMoV12 Si was used as the filler metal in the welding. The GTAW welding process was conducted in a controlled manner and all the parameters used during the process was monitored. The post welding heat treatment was applied in order to eliminate the variations in the hardness of the welded materials. The samples were characterized using tensile, bending, hardness, and notch impact tests. Macro photographs were taken from the samples to observe the transition areas. The results indicated that the mechanical properties obtained from the samples welded in PC position were higher than those obtained from PJ position.

Keywords:
Weld; Welding positions; Mechanical tests; Heat input.

Article History:
Received: 2017/07/24
Accepted: 2017/08/21
Online: 2017/12/28

***Correspondence to**: Bünyamin Çiçek, Hitit University, Alaca Avni Celik Vocational School, Corum, Turkey*
Tel: +90 (364) 411-5050/4515
Fax: +90 (364) 411-5353
E-Mail: bunyamincicek@hitit.edu.tr

INTRODUCTION

Steels with martensitic microstructure (low carbon) and high creep resistance can be used at high temperatures for a long period of time. One of the potential applications of these materials is thermal and nuclear power plants. Over the years, the demand on the service temperature level in these plants have increased. As a result, studies on the development of new steel-based materials with enhanced creep and corrosion resistance have soared. The graph shown in Fig. 1 shows the need for service temperatures and pressures depending on years. Steels with 9-12% Cr content have been started to be used in these applications since 1950s. These steels can be used at the pressures of about 350 bar and temperatures of 600°C. In our work, X20CrMoV11-1 (short name X20) steel was used from these steels. [1, 2]

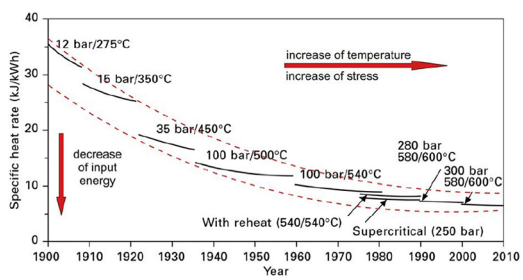

Figure 1. Heat rate of steam power plants in Germany as a function of steam parameters[1]

The X20 steel, developed in 1950, containing 12% Cr, was modified in 1970s by micro-alloying with tungsten. This phase enhances the corrosion and oxidation resistance. The main use of these steels in the world was limited primarily to turbine blades. However, in Europe these modified steels have been used in steam pipelines for energy production especially in Germany. The weldability of this X20 steel was low due to the high carbon content (especially due to the high content of carbon-about 0.2%). The high carbon content results in to hydrogen fracture. On the other hand, these deficiencies were minimized by the heat treatment of the weld zone. This post-weld heat treatment (PWHT) is made to dissipate the irregular hardness distribution in the weld zone [2-5].

In the world, the X20 steel was used in the construction of the indispensable elements in the energy sector. In the application stage, the acceptability of

welding related to the rapid cooling (cooling time and rate) of the weld zone was found to be in different positions [6-10]. In our study, we aimed to unravel the effect of different welding positions on the mechanical and microstructural properties of X20 steel. We tried to shed light on the welding science in the X20 steels depending on various welding configuration.

MATERIALS AND METHOD

In this study, pipes made of X20 steel with the dimensions of Ø38x5 mm were used. According to production reports; the X20 material was exposed to hydrostatic testing at the pressure of 70 bar for 5 sec. Then, a 20 minute normalization heat treatment conducted at 1090°C and tempering heat treatment at 780°C were applied to the samples. The chemical composition of the steel samples determined using spectral analysis method

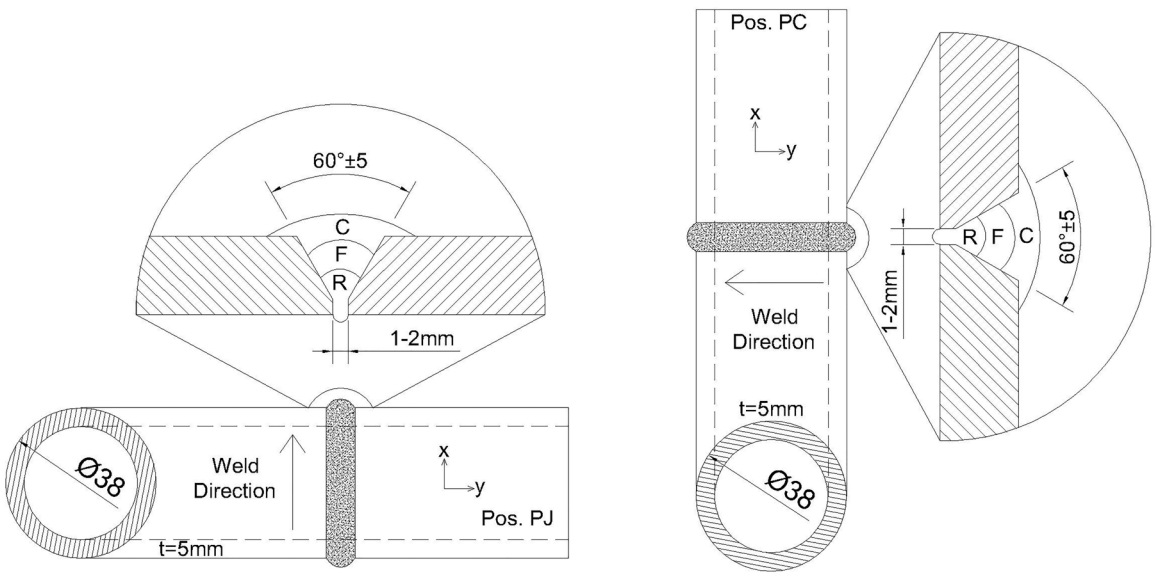

Figure. 2. Welding positions PJ-PC and welding groove details

Table 1. Comparison of chemical composition of 11-12% Cr steels according to to steel makers [2] and Chemical composition of tested X20 steel grade. (Based on the manufacturer's data).

	Chemical Element (%)															*Ceq**
Type	*C*	*Si*	*Mn*	*Nb*	*Co*	*Cr*	*Mo*	*Ni*	*Cu*	*V*	*W*	*B*	*N*	*Ta*	*Nd*	
X20	*0,2*	*0,4*	*0,6*	-	-	*11*	*1*	*0,5*	-	*0,25*	-	-	-	-	-	*1,37*
HCM12A (T/P122)	*0,11*	*0,1*	*0,6*	*0,05*	-	*12*	*0,4*	-	*1*	*0,2*	*2*	*0,003*	*0,03*	-	-	*1,46*
NF12	*0,08*	*0,2*	*0,5*	*0,07*	*2,5*	*11*	*0,2*	-	-	*0,2*	*2,6*	*0,004*	*0,05*	-	-	*1,28*
SAVE12	*0,1*	*0,3*	*0,2*	*0,07*	*3*	*11*	-	-	-	*0,2*	*3*	-	*0,04*	*0,07*	*0,04*	*1,25*
VM12-SHC	*0,12*	*0,5*	*0,3*	*0,055*	*1,6*	*11,5*	*0,3*	*0,25*	-	*0,25*	*1,5*	*0,0045*	*0,05*	-	-	*1,36*
X20 (Tested)	*0,17*	*0,26*	*0,47*	-	-	*10,39*	*0,94*	*0,38*	-	*0,27*	-	-	-	-	-	*1,35*

*C_{eq} *calculated by K. Winterton Formula for pre-heat temp.[13]*

Table 2. Filler Metal Chemical Analysis (EN 21952) (according to the manufacturer's data).

Element	*C %*	*Si %*	*Mn %*	*P %*	*S %*	*Cr %*	*Ni %*	*W %*	*V %*	*Mo %*
min.	*0,170*	*0,200*	*0,400*	-	-	*10,500*	-	*0,350*	*0,200*	*0,800*
max.	*0,240*	*0,600*	*1,000*	*0,025*	*0,020*	*12,000*	*0,800*	*0,800*	*0,400*	*1,200*
W20	*0,199*	*0,46*	*0,6*	*0,015*	*0,001*	*11,03*	*0,34*	*0,4*	*0,31*	*1,01*

Table 3. During of Welding use to Parameters

Pass Code	Current (A) Avg.	Voltage (V) Avg.	Current Type (Filler Metal Polarity)	Weld Speed mm/min. Avg.	Heat Input KJ/mm. Avg.
Root (R)	75	10	DC (-)	52	0,87
Filler (F)	105	11	DC (-)	55	1,26
Cap (C)	115	12	DC (-)	57	1,45

(product data). TIG welding method was used in different welding positions of PC and PJ and the corresponding configurations are shown in Fig. 2. In the same figure, weld groove and pass numbers (R-Root, F-Filler, and C-Cap) are also indicated. The welding processes were carried out by EN 9606-1 certified welders and by taking the considering carbon equivalent (C_{eq}) value into account, the specimens were preheated to 250 °C before the welding [11] (EN 12952-5). As shown in Fig. 2, the welding of the metals were conducted in 3 passes and the inter-pass temperature was measured to be 350-400 ˚C. WCrMoWV12Si (named as W20 throughout the manuscript) was used as filler material. The chemical composition of the filler material is shown in Table 2(acc. to product data). In the table, the composition of a standard filler material is also given to compare the composition of the applied filler with the standards. The welding parameters used in the work is listed in Table 3. The heat input was calculated based on Equation 1 using the values shown in Table 3 [12].

$$H = \frac{60 \text{ x E x A}}{1000 \text{ x S}} \quad (1)$$

where; **H**=heat input(kJ/mm), **E**=arc volt(volts), **A**=current(amp), **S**=weld speed (mm/min)

Heat input is a relative measure of the energy transferred per unit length of the weld. It has a significant effect on the characteristics of the weld metal since it affects preheat and inter-pass temperature. In addition, as a function of heat input, the cooling and heating rate of the metal chances, which in turn results in obtaining different mechanical properties and the metallurgical structures in the weld metal and the HAZ [12]. The welded samples were finally exposed to a post-weld heat treatment (PWHT) based on EN 12952-5 (Table 4). The cycle graphic after the PWHT operation is presented in Fig. 3a and schematic drawn it is given Fig. 3b. The cooling and the heating rates were calculated using the slopes of the graph. The calculated heating and cooling rate values were found to be compatible with the standards values as shown in Table 4 and, PWHT (Post Weld Heat Treatment) parameters for all position specimens.

After the welding process, all the samples were characterized using non-destructive tests (NDT) including

Table 4. PWHT parameters.

Material Group Code (acc. to EN 15608)	Material First Temp. (°C)	Heating Rate (°C/h)	Max. Temp. (°C)	Holding Time (min.)	Cooling Rate (°C/h)	Device* Closed Temp. (°C)
min.	-	-	730	30	-	-
max.	-	150	770	-	400	-
Group No: 6	25	150	750	30	150	175

** Device= PWHT Heater device (Weldotherm STE 82-6)*

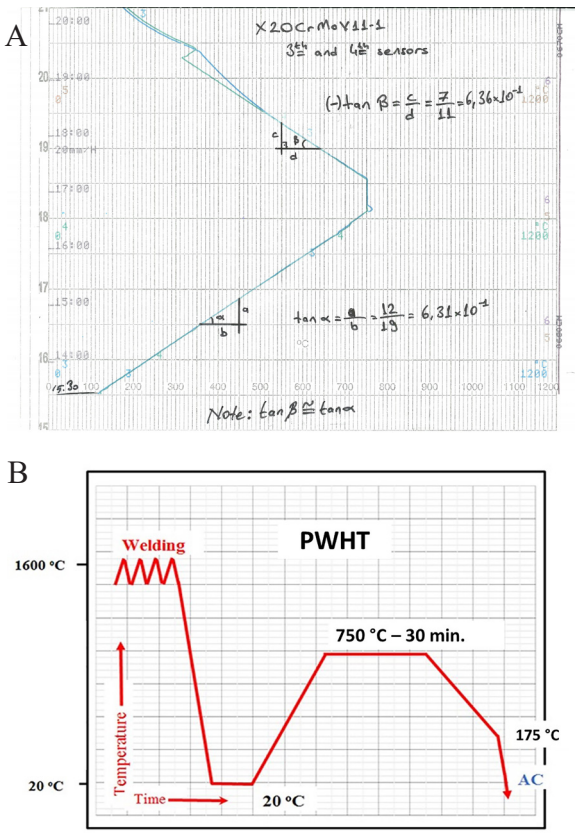

Figure. 3. PWHT graphs for both positions; (a) device, (b) schematic.

visual (VT), penetrant (PT), and radiography (RT) tests. All the mentioned tests were conducted according to the requirements of quality level B in EN 5817. The samples which passed the NDT tests were then subjected to further mechanical testing. The mechanical tests used in the work and their corresponding standards are given below.

1. Tensile Test (made of acc. to EN 4136)
2. Bending Test (made of acc. to EN 5173)
3. Impact Test (made of acc. to EN 9016)
4. Hardness Test (made of acc. to EN 9015-1)
5. Macrostructure Analysis (made of acc. to EN 17639)

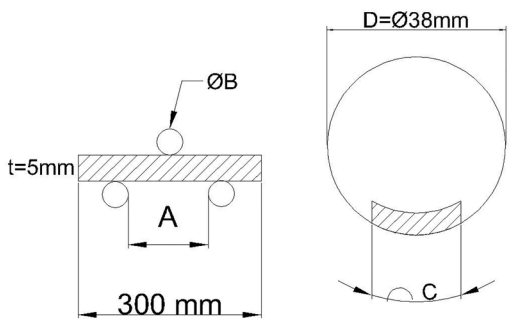

Figure. 5. Bending test parameters according to relevant the standard

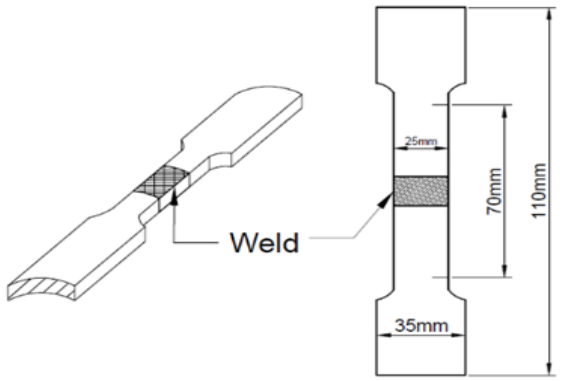

Figure. 4. Tensile test specimen acc. to relevant the standard

Tensile Test

The sample configuration used in the tensile testing is shown in detail in Fig. 4 and used Instron 5989 tensile module. The tests were carried out at room temperature.

Bending Test

The bending test parameters and the applied test method are shown in Fig. 5. Specimens were prepared for two welding positions (PC and PJ), separately for both root and face as required by relevant standard (Fig. 5). The bending values and test parameters were calculated according to the equations given below. The 3-point bending test was conducted using an Instron 5989 Bend Module.

$$A_{min} = D + (2 * t) + 3 \quad (2)$$

$$A_{max} = D + 3t \quad (3)$$

$$B = \frac{100 * t}{E} - t \quad (4)$$

$$C = t + (0.1 * D) \quad (5)$$

Where; **A**: Distance rollers, **B**: Bend roller diameter, **C**: Specimen width, **t**: Thickness, **D**: Pipe diameter

Impact Test

The sample configuration used for impact testing is

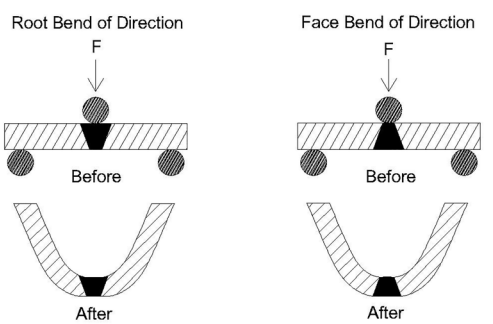

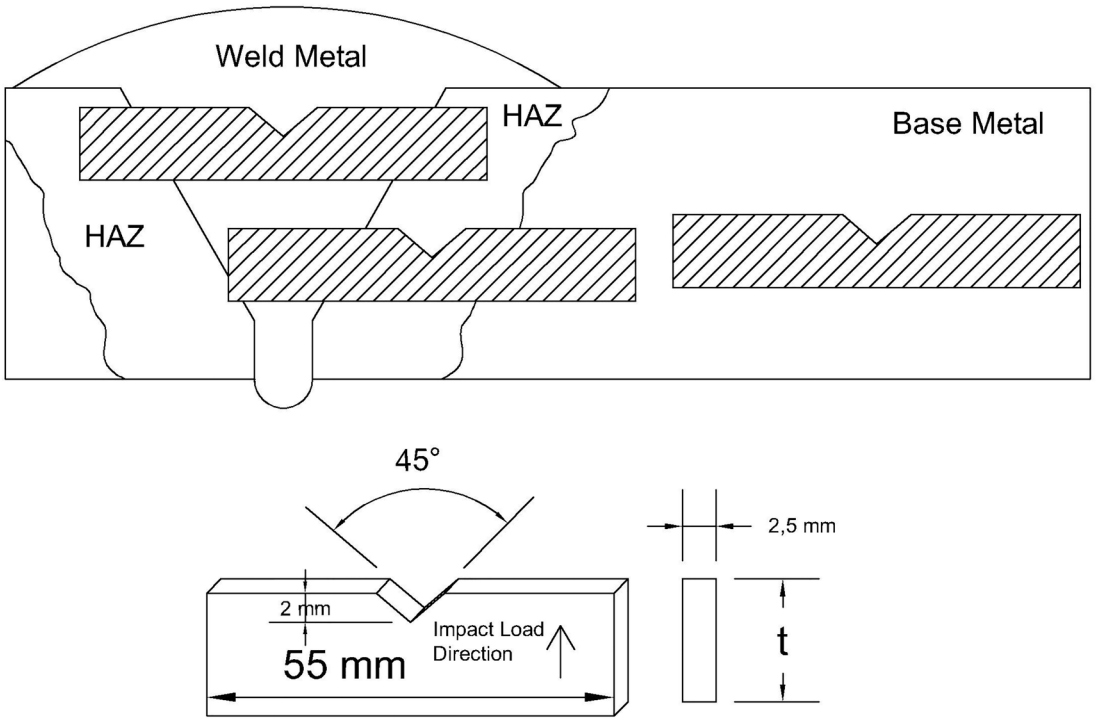

Figure. 6. Dimensions of impact test specimens and notch locations acc. to the standard

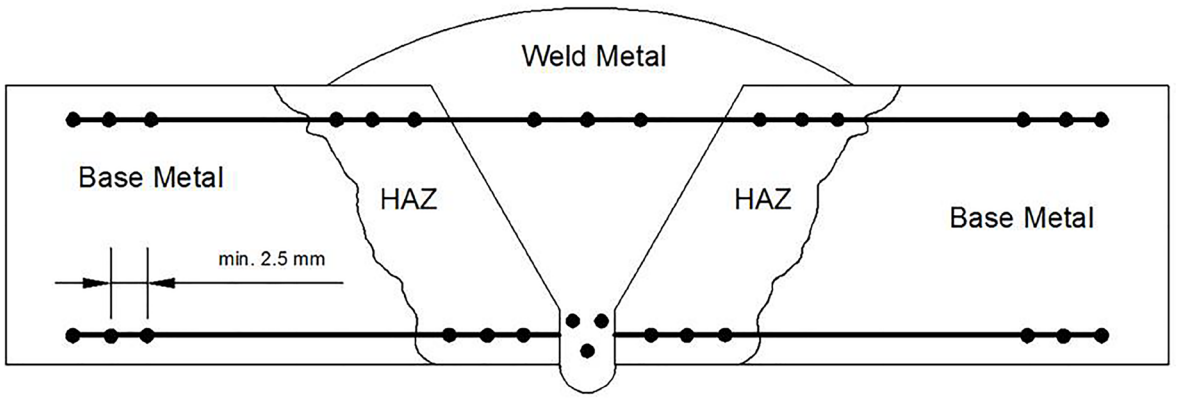

Figure. 7. Measurement locations for hardness test

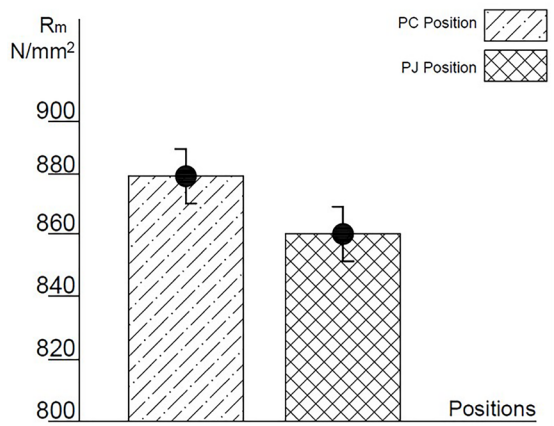

Figure 8. Tensile strength values

shown in Fig. 6. The tests were carried out at room temperature. These specimens were examined with an Instron 450MPX. For each welding positions, 3 specimens were prepared from the base material, HAZ, and weld metal.

Hardness Test

The hardness tests were conducted at the root line and cap line (Fig. 7) using 10 kg of load used to Vickers (HV10). These specimens were examined with a Qness Q10M. 3 independent measurements were recorded at the root and cap line.

Macrostructure Analysis

Specimens were cut from the vertical section of welded

Table 5. Tensile Test Results

Specimen Code	Test Temp. (ºC) (+)	Max. Load (kN)	Rp 0,2 (N/mm²)	Rm (N/mm²)	Elongation (%)
PC 1	20	103	657	882	16,3
PC 2	20	104	685	876	16,9
PJ 1	20	99	630	861	17,1
PJ 2	20	96	633	857	16,2

plates in order to investigate the welding zone. The samples were made of metallographic process and etched with a Nital10 solution (%10 HNO3 + %90 Alcohol) [14, 15].

RESULTS AND DISCUSSION

It is known that the weld quality requires control of weld pool width and cooling time. The cooling time $t_{8/5}$ (from 800 °C to 500 °C) is related to the hardness of the weld metal [16]. The microstructure of the weld metal is highly dependent upon speed of the heating and cooling cycles and based on these parameters various microstructural features are formed in the weld metal. Therefore, one of the most important factors affecting the microstructure and thus strength of the weld metal is the cooling time which is the function of the heat input [16]. The weld regions of carbon steels mainly consists of a microstructure containing allotriomorphic ferrite grains (primary ferrite or grain boundary ferrite – α_a), acicular ferrite (AF), and Widmanstatten ferrite (ferrite with aligned second phase – α_W) phases [17-20].

Tensile Test

The tensile test results showed that all the specimens got broken in the HAZ area. Tensile strength (Rm) of the samples which were welded in PC position was higher than those obtained from welded samples in PJ position. The results revealed that the highest tensile strength (879 N/mm²) was obtained from the sample welded in PC position. The tensile strength of the sample welded in PJ position, however, was found to be 859 N/mm² (Fig. 8). The all of results in the test is listed in Table 5. Despite the difference between the tensile strength values, elongation of the samples were close to each other. In addition, as expected from EN10216-2: A1 standards, the elongation should began in range of 14-17% which is fully compatible with the test results.

It was reported that while the welding position of a metal did not have any significant effect on tensile and hardness values, the toughness of the weld metal showed a dependency on the welding position [21]. It was observed that the toughness value of the weld metal obtained from the vertical position was lower than that of obtained from the flat position at all temperatures. In the same paper it was also shown that the hardness values obtained regardless of the welding positions were close to each other, indicating a good agreement with the tensile test results [21]. Those findings suggest that the total heat input values can be different in each material during the welding process. The difference in the total heat input value varying based on the welding position leads to different cooling rate and time, which in turn results in the formation of different grain structure and microstructure [16]. The difference in the cooling rates, as well as the dwell time at high temperatures causes significant microstructural changes [22]. Briefly; the difference in the mechanical properties of the weld metal is attributed to the difference in the cooling time (t8/5) resulted from the amount of heat input.

Bending Test

The bending test parameters and results are shown in Table 6. Images taken random from the bended samples are given in Fig. 9 for both root and face bending. It is noteworthy that after both bending modes, no crack formation was observed in welding and HAZ regions. After the bending tests, no visual damage was observed after 180° folding. Furthermore, liquid penetration test detected no invisible surface cracks. The PC and PJ

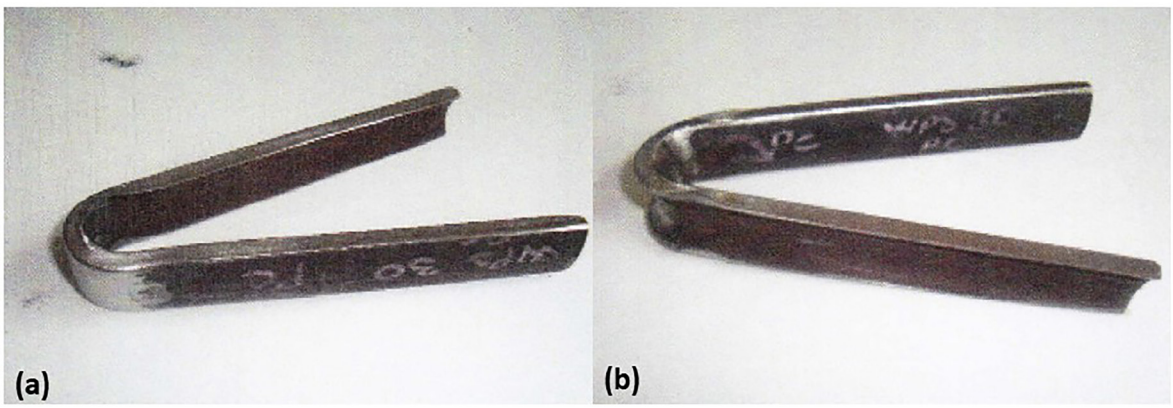

Figure. 9. Bending test sample type photos; (a) Face bend, (b) Root bend

Table6. Bending Test Results

Test Specimen Code	Test Direction*	Rollers Distance (A) (mm)		Roller Diameter (B) (≈mm)	Specimen Width (C) (≈mm)	Last Bending Angle	Crack Result*
		min	max				
PC	F	51	52	24	9	180°	UN
PC	R	51	52	24	9	180°	UN
PJ	F	51	52	24	9	180°	UN
PJ	R	51	52	24	9	180°	UN

** F = Face Bend, R = Root Bend, UN = Unobserved*

positions no damage was reported neither in weld metal nor in HAZ. In a study conducted by Figueirôa et al. [6] showed that weld region with a lower shape factor and more penetration were observed. In addition, when the same test but in the overhead position was applied to the same material the authors obtained weld regions with

a low shape factor [6]. Our results (shown in Fig. 7) indicated a low shape factor and thus no deformation, which is in a good agreement with the results shown by Figueirôa et al. [6].

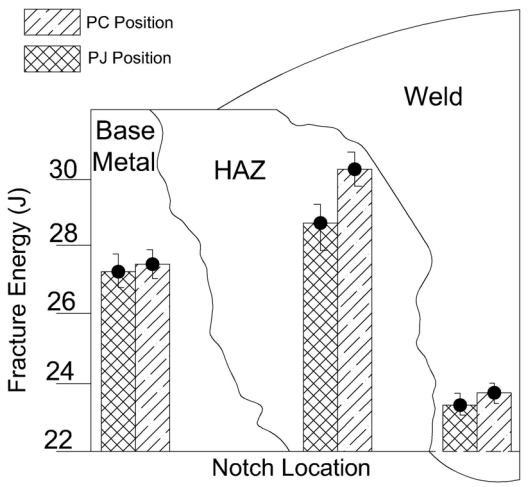

Figure. 10. Fracture energy difference of zones

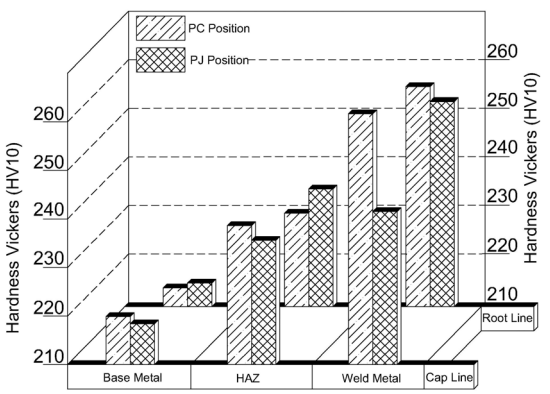

Figure. 11. Hardness test results

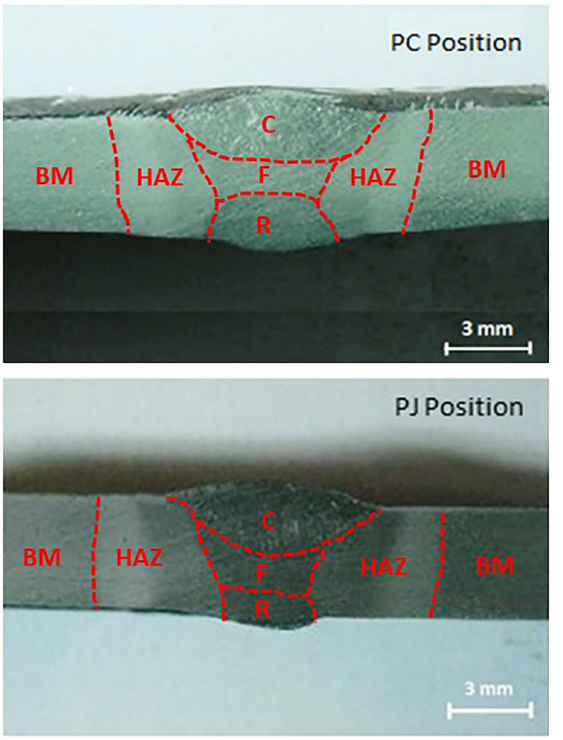

Figure. 12. Macrostructure images

Impact Test

Impact test results are shown in Fig. 10. For the specimens welded in PC position, the fracture energy values of 27, 31, and 23 J were obtained from the base, HAZ, and weld metal, respectively. For the samples welded in PJ position, the measured fracture energy values were 27, 29, and 23 J in base, HAZ, and weld metal, respectively.

When the Charpy test results are taken into account, it can be stated that welding position had no effect on the fracture energy. The toughness of the HAZ area, however, was higher than the toughness values obtained from both weld and base metals. Gomes et al. [22] explained the increment in the toughness in the HAZ area by the repeated welding process in the HAZ region. The repeated welding process results in a recrystallization of the HAZ region in every welding pass, which in turn leads to higher toughness [22].

Hardness Test

The results are given in Fig. 11. It is expected that hardness of the weld metal should be higher than the base metal and HAZ, which was confirmed by this study. For every welding positions, the base metal hardness values were 211±9 HV min. and 220±5 HV max. as shown in Figure 11. Hardness values of HAZ were 211±9 HV min. and 238±7 HV max. On the other hand, measurements on weld metal were found to be 244±5 HV min. and 264±6 max.

The hardness test results indicated that for both welding modes, the hardness of the base metal was different than those obtained from weld metal. In addition, the welding process resulted in an increase in the hardness. This can be explained by cooling time and fine grain structure of the weld metal. Heat input that transferred into the material during the welding process caused hardening in HAZ and weld metal. Hardness values measured from the base metal and HAZ were close to each other. However, hardness of the weld metal measured in the cap line were higher for PC and lower for PJ. The values in the root of the weld metal were about the same level. For PC position, this can be explained by the effect of the total heat input on grains. When the cooling is faster because of the lower total heat input, the structure will be harder. Finally, looking at all the values, the maximum 350 HV (HV10) limit in EN12952-6 standard was not exceeded [23-25]. The highest hardness values were measured in the HAZ and weld metal, and can be attributed to the process of quenching and tempering by the subsequent passes. This hardening only occurs in steels in which a small fraction of martensitic microstructure is formed and when they possess elements that promote secondary hardening [26-28].

Macrostructure Analysis

The images of the welding zone shown in Fig. 12 recorded by a Strues-Welding Expert. The images were taken using the standard of EN 17639.

Macro images (BM: Base Metal) of the side surfaces were examined for both welding modes at different positions. Root (R), filler (F), and cap (C) formations were observed from the images. HAZ also occurred because of the heat input. HAZ showed equal distribution on both sides of welding depending on the heat input for both positions. No defect or discontinuities were detected from the weld metal to HAZ transition area. Similarity; a study, macro photographs taken and HAZ borders were examined. But because the preheat value varies in this study, the HAZ limits are different and the other areas (base metal and weld metal) are clearly monitored [22]. In our work, the HAZ limits are close to each other because the preheat value is constant.

CONCLUSION

In our work, the effect of welding position on the mechanical properties of weld metals (X20CrMoV11-1 steels (X20)) were evaluated. The obtained results are given below:

1. Similar tensile test results were obtained regardless of the welding position, which is consistent with the literature.
2. It was observed that the bending behavior of the weld metal was not affected by the welding position. No deformation was observed in the weld zone for both positions.
3. The impact test results indicated that the toughness values obtained from the HAZ region were higher than the toughness values measured from the welding zone and base metals. In addition, the toughness of the weld zone was low due to the high hardness of the region. The toughness of the base metal was similar with the data obtained during the fabrication process of the metal.
4. The Vickers test results confirmed the impact test results and were in a good agreement with the literature.
5. Macro photographs taken from the weld zone showed all the elements of the welding zone and there was no difference based on the welding position.

REFERENCES

1. Bazazi, A.A., Evolution of Microstructure during Long-term Creep of a Tempered Martensite Ferritic Steel. 2009: Cuvillier.
2. Urzynicok, M., K. Kwieciński, and M. Szubryt, Experience in the welding of martensitic steel VM12-SHC. Welding International, 2013. 27(4): p. 249-254.
3. Qian, Y. and J. Zhao, Influences of local PWHT from different criteria at home and abroad on the residual stress of the under-matching welded joint. International Journal of Pressure Vessels and Piping, 2017. 154: p. 11-16.
4. Khalaj, G., Pouraliakbar, H., Jandaghi M.R., Gholami A. Microalloyed steel welds by HF-ERW technique: Novel PWHT cycles, microstructure evolution and mechanical properties enhancement. International Journal of Pressure Vessels and Piping, 2017(152): p. 15-26.
5. Loots, R., Susceptibility of service exposed creep resistant materials to reheat cracking during repair welding, University of Pretoria, 2003.
6. Figueirôa, D.W., Pigozzo, I.O., Gonçalves e Silva, R.H., Abreu Santos T.F., Filho S.L.U. Influence of welding position and parameters in orbital tig welding applied to low-carbon steel pipes. Welding International, 2017. 31(8): p. 583-590.
7. Muzaka, K., Park, M., Lee, J.P., Jin, B., Lee B.R., Soo Kim, W.Y. A Study on Prediction of Welding Quality Using Mahalanobis Distance Method by Optimizing Welding Current for A Vertical-position Welding. Procedia Engineering, 2017. 174: p. 60-67.
8. Yan, Z., Xu, D., Li, Y. A visual servoing system for the torch

alignment to initial welding position. Intelligent Robotics and Applications, 2008: p. 697-706.
9. Bermejo, M.V., Karlsson L., Svensson, L.E., Hurtig, K., Rasmuson, H., Frodigh, M., Bengtsson, P., Effect of welding position on properties of duplex and super duplex stainless steel circumferential welds. Welding in the World, 2015. 59(5): p. 693-703.
10. Pasternak, J., S. Fudali, Własności oraz doświadczenia w spawaniu stali przeznaczonych na elementy ciśnieniowe kotłów o parametrach nadkrytycznych. XVI Międzynarodowa Konferencja Spawanie w Energetyce, Opole-Jarnołtówek, 2008.
11. Yurioka, N., T. Kasuya, A chart method to determine necessary preheat in steel welding. Welding in the World/Le Soudage dans le Monde, 1995. 5(35): p. 327-334.
12. Funderburk, R.S., A look at input. Welding Innovation, 1999. 16(1).
13. Rao, T.R., Metal casting: Principles and practice, New Age International, 2007.
14. Kurgan, N., Sun, Y., Cicek, B., Ahlatci, H., Production of 316L stainless steel implant materials by powder metallurgy and investigation of their wear properties. Chinese science bulletin, 2012. 57(15): p. 1873-1878.
15. Vander Voort, G.F., Etching isothermally treated steels. Heat Treating Progress, 2001. 1(2): p. 25-32.
16. Jin, B., M. Soeda, K. Oshima, Control of weldpool width and cooling time in TIG welding using a neural network model. Welding international, 1996. 10(8): p. 614-621.
17. Grong, O., D.K. Matlock, Microstructural development in mild and low-alloy steel weld metals. International Metals Reviews, 1986. 31(1): p. 27-48.
18. SA, D., Inclusion formation and microstructure evolution in low alloy steel welds. ISIJ international, 2002. 42(12): p. 1344-1353.
19. Hu, F., P. Hodgson, K. Wu, Acceleration of the super bainite transformation through a coarse austenite grain size. Materials letters, 2014. 122: p. 240-243.
20. Santos,T.F., Torres, Edwar A. Vilela, José M. C. Andrade, Margareth S. Cota, André B., Caracterização Microestrutural De Aços Baixo Carbono Por Microscopia De Força Atômica (Microstructural Characterization Of Low Carbon Steels By Atomic Force Microscopy). Revista Latinoamericana de Metalurgia y Materiales, 2014: p. 118-133.
21. Masoumi, F., D. Shahriari, Effects of welding positions on mechanical properties and microstructure in weld metal of high strength steel, Advances in Materials and Processing Technologies 83(2009) p. 1121-1127.
22. Gomes Moojen, R., Machado, I.G., Mazzaferro J.A.E., Gonzalez, A.R., Cooling rate effects in the welding of API 5L-X80 steel. Welding International, 2017. 31(2): p. 100-110.
23. Kasuya, T., N. Yurioka, M. Okumura, Methods for predicting maximum hardness of heat-affected zone and selecting necessary preheat temperature for steel welding. Nippon Steel Technical Report, 1995: p. 7-14.
24. Graville, B., Weld Cooling Rates and Heat-Affected Zone Hardness in a C Steel. Welding Journal, 1973. 52(9): p. 377-385.
25. Abd El-Rahman Abd El-Salam, M., I. El-Mahallawi, M. El-Koussy, Influence of heat input and post-weld heat treatment on boiler steel P91 (9Cr–1Mo–V–Nb) weld joints Part 1–Microstructure. International Heat Treatment and Surface Engineering, 2013. 7(1): p. 23-31.
26. Kim, C.M., J.B. Lee, J.Y. Yoo. A study on the metallurgical and mechanical characteristics of the weld joint of X80 Steel. The Fifteenth International Offshore and Polar Engineering Conference. , 19-24 June, Seoul, Korea, p. 158-162, 2005.
27. Zhu, Z., Structure property correlation in the weld HAZ of high strength line pipe steels, University Of Wollongong Thesis Collection, 2013.
28. Nicholas, J., Abson. The prediction of maximum HAZ hardness in various regions of multiple pass welds, 17th International Conference Computer Technology in Welding and Engineering, University of Cranfield, 18-19 June, 2008.